Energy & Environmental Science

Accepted Manuscript

ROYAL SOCIETY OF CHEMISTRY

www.rsc.org/ees

Energy & Environmental Science

RSCPublishing

ARTICLE

Non-precious Metal Electrocatalyst with High Activity for Hydrogen Oxidation Reaction in Alkaline Electrolytes

Cite this: DOI: 10.1039/x0xx00000x

Received 00th January 2012,
Accepted 00th January 2012

DOI: 10.1039/x0xx00000x

www.rsc.org/

Wenchao Sheng,[1] Adam P. Bivens,[1] MyatNoeZin Myint,[1] Zhongbin Zhuang,[1] Robert V. Forest,[1] Qianrong Fang,[1] Jingguang G. Chen,[2,3,*] and Yushan Yan[1,*]

Abstract: A ternary metallic CoNiMo catalyst is electrochemically deposited on a polycrystalline gold (Au) disk electrode using pulse voltammetry, and characterized for hydrogen oxidation reaction (HOR) activity with temperature-controlled rotating disk electrode measurements in 0.1 M potassium hydroxide (KOH). The catalyst exhibits the highest HOR activity among all non-precious metal catalysts (e.g., 20 fold higher than Ni). At a sufficient loading, the CoNiMo catalyst is expected to outperform Pt and thus provide a promising low cost pathway for alkaline or alkaline membrane fuel cells. Density functional theory (DFT) calculations and parallel H_2-temperature programmed desorption (TPD) experiments on structurally much simpler model alloy systems show a trend that CoNiMo has a hydrogen binding energy (HBE) similar to Pt and much lower than Ni, suggesting that the formation of multi-metallic bonds modifies the HBE of Ni and is likely a significant contributing factor for the enhanced HOR activity.

Introduction

Low-temperature hydrogen proton-exchange membrane fuel cells (PEMFCs) with high power density have been developed as an efficient and environmentally friendly energy conversion device for a future clean and sustainable energy system.[1-3] However, the commercialization of PEMFCs has long been hampered by the lack of a highly efficient and cost-effective oxygen reduction reaction (ORR) catalyst. At present, the state-of-the-art ORR catalyst for PEMFCs is Pt, which even at its current unacceptably high loading still has a cell voltage loss of 300 mV~400 mV under typical operation conditions.[4] The greatest challenge for the development of an inexpensive ORR catalyst is that most non-precious metals and alloys are unstable in acid and thus face long term durability issues in PEMFCs.[5, 6] Recently several exciting non-precious metal ORR catalysts have been shown to have activity comparable to that of Pt,[7, 8] but their long term durability in acid remains to be proven. As an alternative to PEMFCs, liquid alkaline or alkaline membrane fuel cells (AFCs/AMFCs) are attractive because non-precious metals and alloys in general are much more stable in base than in acid. Non-precious metal ORR catalysts with an activity similar to that of Pt have been reported in base including Fe-based macrocycles,[9] nitrogen doped carbon nanotube/nanoparticle composite[10] and Perovskite oxides.[11] However, a serious concern on the anode side, i.e., the hydrogen oxidation reaction (HOR), arises when switching from an acidic to alkaline medium. As demonstrated by previous studies, the HOR activity in base on the most active catalyst, Pt, is two orders of magnitude smaller than in acid, which in turn requires higher Pt loading on the anode.[12, 13] Although PtRu alloy has been found to have enhanced HOR activity over Pt in a recent study,[14] the discovery of highly active non-precious HOR electrocatalysts in base is crucial in order to make AFCs/AMFCs practical.

Ni-based materials are the most commonly used non-precious metal electrocatalysts for H_2 production (HER) in alkaline electrolysers[15-20] and the HOR in AFCs.[21, 22] Several Ni-based bimetallic catalysts including Cr,[23] Ti,[24] La,[25] Cu,[26] and Mo,[27-29] and a ternary Ni-Mo-Fe alloy[19] have been developed to increase the HOR activity. However, the enhancement of the HOR on Ni alloy over that on Ni is very limited, and the mechanism behind the improvement has been vague. A previous study has shown that decorating Ni with Cr can tune the Ni d-band structure and in turn weaken the Ni-O bond so that metallic Ni surface becomes available for the HOR.[30] In this paper, we prepared NiMo and CoNiMo electrocatalysts by electrodeposition and studied their HOR activity in 0.1 M KOH using temperature controlled rotating disk electrode method. The electroplated NiMo and CoNiMo multi-metallic catalysts exhibited significantly enhanced HOR activity over electroplated Ni catalyst in KOH electrolyte (20 times). To qualitatively understand the HOR activity trend, we performed density functional theory (DFT) calculations and parallel H_2-temperature-programmed desorption (H_2-TPD) experiments on structurally much simpler alloy systems that are more accessible to DFT calculations and TPD experiments. Our results suggest that a weakened hydrogen binding energy (HBE) is a significant contributing factor for the improved HOR on multi-metallic NiMo and CoNiMo catalysts.

Experimental Section

Electrodeposition of CoNiMo

The electroplating setup was assembled of a 100 mL polypropylene cell, a double-junction Ag/AgCl reference electrode (Pine Instruments), and a graphite rod (Alpha Aesar) counter electrode. The RDE working electrode was brought to 3600 rpm and the plating solution was continually purged with H_2 gas. The final solution was composed of 0.248 M $NiSO_4$ (98% purity, Alfa Aesar), 0.049 M Na_2MoO_4 (98% purity, Aldrich), 0.006 M $CoSO_4$ (98% purity, Alfa Aesar), and 0.216 M trisodium citrate ($Na_3C_6H_5O_7$, 98% purity, Sigma). The electroplating procedure began with oxidizing the Au disk surface at 0.8 V vs. Ag/AgCl for 2 minutes to remove impurities. The potential was then pulsed for 50 ms at a plating potential of −2.1 V vs. Ag/AgCl and held for 500 ms at the resting potential of −0.6 V vs. Ag/AgCl for a total deposition time of 14 minutes. The electrode was then removed from the plating bath and rinsed with care to keep the surface submerged at all times, given that the oxide forms with extended exposure to air.

Electrochemical characterization

Steady state rotating disk electrode (RDE) measurements for HOR/HER were made in H_2-saturated 0.1 M KOH (99.99% metal purity, Sigma Aldrich) solution in a jacketed glass cell with circulating water temperature control (Pine Instrument), against a double-junction Ag/AgCl reference electrode (Pine Instrument), with a platinum wire (Pine Instrument) as the counter electrode. The sample was reduced at −2.00 V vs. Ag/AgCl for 2 minutes to remove residual oxides from air exposure. In order to remove the large capacitive current background within the same potential range as the HOR, the steady state measurements were used to observe the HOR and HER activities rather than cyclic voltammetry. Currents were measured after 15 seconds holding at potentials with a 5 mV voltage interval from −1.75 V to −0.85 V vs. Ag/AgCl, at 1600 rpm at 274 K, 283 K, 293 K, 303 K and 313 K. However, the potential was reported with respect to the RHE scale, if not specified otherwise. HOR/HER on Au in H_2-saturated 0.1 M KOH were also measured using RDE method and no HOR activity near the reversible hydrogen potential was observed as shown in Fig. S3.

Cell resistance was measured after each experiment using the AC impedance spectra taken between 1 Hz and 200 kHz. The voltage was kept at a constant potential with a 10 mV voltage perturbation. The real part at 1 kHz was used as the cell resistance value to obtain the iR-free polarization curves.[13] The cell resistances were determined to be 53 Ω at 274 K and 26 Ω at 313 K.

Density functional theory (DFT) calculations

The DFT binding energies of atomic hydrogen were calculated using the Vienna *ab initio* Simulation Package (VASP).[31, 32] The exchange-correlation energy was approximated using the PW91 functional within the generalized gradient approximation (GGA) with a basis set of plane waves up to an energy cutoff of 396 eV. In all cases, the model surface consisted of a periodic 3 × 3 unit cell with four layers of metal atoms at the corresponding most closed-packed surfaces separated by six equivalent layers of vacuum. The two bottom layers of the slab were fixed. During hydrogen binding energy calculations, the top two metal layers and the adsorbed hydrogen atom were allowed to relax to reach the lowest energy configuration. The Ni/Mo(110) surface was modified by replacing all Mo atoms from the top layer with Ni atoms. The Ni-Co-modified Mo(110) surface was prepared by replacing a third of Mo atoms from the top layer with Co atoms and the rest from the top layer with Ni atoms. While it is not uncommon to have surface intermixing or subsurface alloying in multi-metallic systems, the highly favorable surface segregation energy of Ni or CoNi on Mo suggests that pseudomorphic overlayer of Ni and Co on Mo(110) is a good representation of the surfaces measured experimentally. A 3×3×1 Monkhorst-Pack k-point mesh was used. Spin-polarization was included for all surfaces. Binding energy was calculated using equation 1[33]

$$E^{H}_{atomic} = E_{H-slab} - E_{slab} - 0.5 * E_{H2(g)} \quad (1)$$

where E^{H}_{atomic} is the binding energy of atomic hydrogen on the given slab, E_{H-slab} is the energy of the slab with 1/9 monolayer (ML) hydrogen adsorbed, E_{slab} is the energy of the slab in vacuum, and $E_{H2(g)}$ is the energy of hydrogen in the gas phase. For all possible binding sites calculated, only the value corresponding to the most stable binding site is reported.

The main objective of the DFT calculations is to determine how hydrogen binding energy is modified by the formation of Ni-Mo and Co-Mo bonds. Due to the structural complexity of the polycrystalline samples in electrochemical measurements, DFT calculations were performed on close-packed surfaces of single crystals, i.e., close-packed (111) facet of the fcc structure, Ni(111), Pt(111), and the (110) facet of the bcc structure, Mo(110), Ni/Mo(110), and CoNi/Mo(110). Another advantage of performing DFT calculations on single crystal surfaces is that the predicted trend can be verified experimentally using H_2-TPD.

Results and discussion

Rotating disk electrode method was employed to evaluate the HOR performance. As illustrated in Fig. 1a, electroplated Ni exhibits little HOR activity while NiMo shows significantly increased HOR activity. The activity of NiMo can be further enhanced with Co electroplated simultaneously. The HOR activity appears highly dependent on the atomic ratio between Co and Ni in the plating solution (Fig. 1b and Table S1). The CoNiMo electroplated from the precursor solution containing Co, Ni and Mo with an atomic ratio of 0.12 : 5.10 : 1.00 showed the highest HOR activity and was used to conduct more detailed kinetic analyses. The HOR polarization curve of polycrystalline Pt disk is also presented in Fig. 1a as a benchmark of HOR performance.

Temperature-dependent HOR/HER performance on CoNiMo was evaluated at 274, 283, 293, 303 and 313 K. Fig. 1c shows the steady state HOR/HER polarization curves of CoNiMo in H_2-saturated 0.1 M KOH at 1600 rpm at selected temperatures with the HOR/HER polarization curves of Pt as a benchmark under the same conditions. The HOR currents on both CoNiMo and Pt increase with applied overpotential below ~0.1 V. After 0.1 V, the HOR currents on Pt continue to increase and reach the limiting currents at ~0.2 V. However, after an initial increase in the HOR currents below 0.1 V, the HOR currents on CoNiMo start to decrease at overpotentials higher than 0.1 V, which is most likely due to the passivation of Ni species on the catalyst surface, as suggested in a previous study.[27] Therefore, the HOR cannot reach the theoretical limiting currents at 274 K and 293 K. Nevertheless, the HOR rate is significantly enhanced at 313 K so that the HOR current on CoNiMo levels off at the HOR limiting current at 0.1 V while the HOR current on Pt disk does not reach the HOR plateau until 0.2 V. The kinetic currents (i_k) of the HOR on CoNiMo and Pt at all temperatures were calculated using the Koutecky-Levich equation[34]

$$\frac{1}{i} = \frac{1}{i_k} + \frac{1}{i_D}$$

where i is the measured current and i_D is the diffusion limited current, and plotted as a function of overpotential in Fig. 1d.

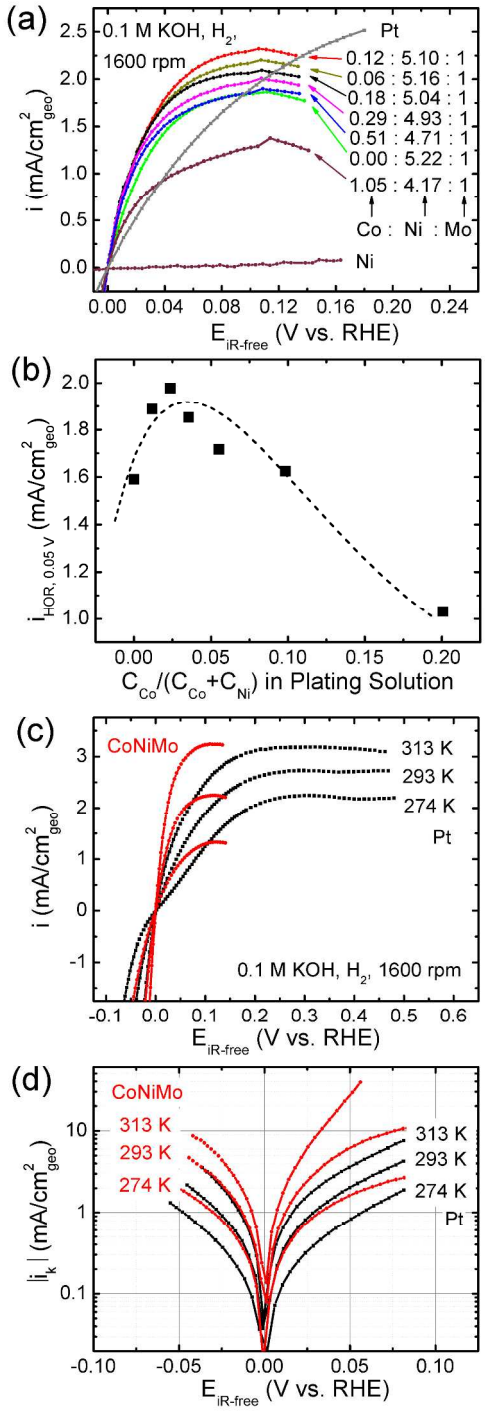

Figure 1. (a): Steady state polarization curves of the HOR/HER on electroplated Ni, NiMo, CoNiMo and polycrystalline Pt disk. The ratio by each curve refers to the atomic ratio between Co, Ni and Mo in the plating solution; (b): the HOR currents at 0.05 V vs. RHE as a function of the $C_{Co}/(C_{Co}+C_{Ni})$ in the plating solution. The polarization curves were collected in H_2-saturated 0.1 M KOH and with a rotating speed of 1600 rpm at room temperature; (c): steady state polarization curves of the HOR/HER on electroplated CoNiMo alloy (red) and Pt disk (black) at 274, 293 and 313 K. (d): kinetic currents of the HOR/HER on CoNiMo (red) and Pt (black) at 274, 293 and 313 K. The HOR kinetic currents were acquired using the Koutecky-Levich equation.

The kinetic currents of the HOR/HER were subsequently fitted to the Butler-Volmer equation[34] to obtain exchange current

$$i_k = i_0\left(e^{\frac{\alpha_a F}{RT}\eta} - e^{\frac{-\alpha_c F}{RT}\eta}\right)$$

where i_0 is the exchange current, α_a and α_c are transfer coefficients for the HOR and HER, respectively, F is the Faraday's constant (96485 C/mol), R is the universal gas constant (8.314 J/mol/K), T is temperature, and η is the overpotential. As suggested in the previous study, the HOR kinetic current calculated using the Koutecky-Levich equation from measured current (i) below 80% of the limiting current was used in order to minimize the errors in the analysis.[13] The best fitting of the HOR/HER kinetic currents on Pt can be obtained with transfer coefficients $\alpha_a=\alpha_c=0.5$ at all examined temperatures (Fig. S1), which suggests that the HOR and HER are symmetric with respect to the reversible hydrogen potential and the one-electron transfer (either Volmer or Heyrovsky step) could be the rate-determining step.[35] However, CoNiMo has a much narrower potential window for the data fitting (< ±40 mV), therefore it could not be exclusively determined whether $\alpha_a+\alpha_c=1$ or $\alpha_a+\alpha_c=2$ applies as both fit to the Butler-Volmer equation fairly well (Fig. S1). Consequently, it is difficult to determine the reaction mechanism of the HOR/HER on CoNiMo at present. Nevertheless, the fitting results show that $\alpha_a\approx\alpha_c$, suggesting that the HOR and HER on CoNiMo are also symmetric with respect to the reversible hydrogen potential, similar to Pt. The exchange current density, obtained through normalization of the total exchange current by the electrochemical surface area of CoNiMo and Pt (Supporting Information, Fig. S2) at 293 K are listed in Table 1. The i_0 of HOR/HER on Pt is determined to be 0.61±0.05 mA/cm^2_{Pt}, which is in excellent agreement with the previous study.[13] The i_0 of the HOR/HER on CoNiMo varies from 0.007±0.001 to 0.015±0.002 mA/cm^2_{Ni}, depending on the fitting parameter ($\alpha_a+\alpha_c$). Because Ni alone barely shows any HOR activity in the vicinity of the hydrogen reversible potential, it is not practical to extract the exchange current density of Ni at 0 V vs. RHE. Therefore, the kinetic current densities of Ni and CoNiMo at 0.05 V vs. RHE are calculated and listed in Table 1 for comparison. CoNiMo shows 20 times higher HOR activity than Ni at 0.05 V vs. RHE, suggesting a significant improvement due to the addition of Co and Mo elements.

Table 1. The HOR/HER exchange current densities and kinetic activities at 0.05 V vs. RHE on Pt disk, CoNiMo and Ni at 293 K and activation energies.

	i_0 (mA/cm^2_{metal})	$i_{k,0.05V}$ (mA/cm^2_{metal})	E_a (kJ/mol)
Pt disk	0.61±0.05	1.44±0.13	29±1
CoNiMo	0.015±0.002 ($\alpha_a+\alpha_c=1$) 0.007±0.001 ($\alpha_a+\alpha_c=2$)	0.044±0.005	35±1 ($\alpha_a+\alpha_c=1$) 36±1 ($\alpha_a+\alpha_c=2$)
Ni	-	0.002	-

Exchange currents of the HOR/HER on CoNiMo and Pt at different temperatures were further plotted as a function of 1/T as shown in Fig. 2. The activation energies of the HOR/HER on CoNiMo and Pt, determined from the Arrhenius plot, were 35±1 kJ/mol and 29±1 kJ/mol, respectively. It should be pointed out that although CoNiMo deactivates at higher overpotentials (> 0.1 V) at

lower temperatures from 274 to 293 K, probably due to surface passivation, the kinetics of the HOR on CoNiMo increases dramatically as the temperature increases such that the HOR current reaches the limiting current before the potential runs into the catalyst passivation regime (Fig. 1c). It is anticipated from the Arrhenius plot (Fig. 2) that the HOR activity should continue to increase with the temperature rising up to 353 K, which is the typical fuel cell operation temperature.

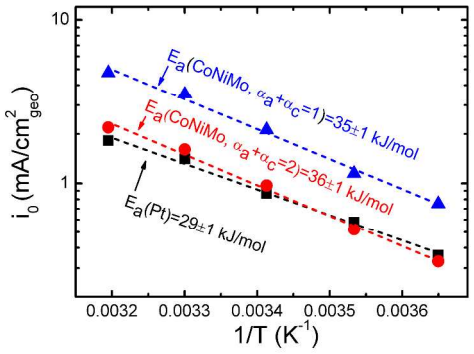

Figure 2. Arrhenius plots of the exchange current of CoNiMo and Pt as a function of 1/T.

The CoNiMo with the best HOR performance was also characterized using scanning electron microscopy (SEM), energy-dispersive spectroscopy (EDS), high-resolution transmission electron microscopy (HRTEM), and glancing incidence X-ray diffraction (GIXRD, Fig. 3, see Supporting Information for experimental details). The SEM image (Fig. 3a) shows that CoNiMo thin layer has a very similar rough surface morphology as those prepared using electrochemical deposition in the previous study.[36] The TEM image (Fig. 3b) reveals that the catalyst is composed of small nanocrystals while the HRTEM measurements (Fig. 3b, inset) show a lattice spacing of 0.20 nm (corresponding to CoNiMo (111) planes). The analysis of GIXRD pattern of CoNiMo (Fig. 3c) shows that CoNiMo (111) peak (43.9 °) is slightly shifted to a lower angle compared to the Ni (111) peak (44.3 °), suggesting that CoNiMo alloy maintains the Ni-like fcc structure. This result is consistent with the HRTEM in terms of d-spacing and the elemental analysis, whereby Ni is found to be the majority (Fig. 3d). The chemical composition of the deposited film was also examined by inductively coupled plasma atomic emission spectroscopy (ICP-AES) and a mass of 3 µg Co, 80 µg Ni, and 29 µg Mo was obtained giving an atomic Co:Ni:Mo=0.17:4.49:1 and again suggesting that Ni is the dominating component of the ternary metallic catalyst. The average thickness of the CoNiMo layer was estimated to be ~0.6 µm from the ICP-AES elemental composition.

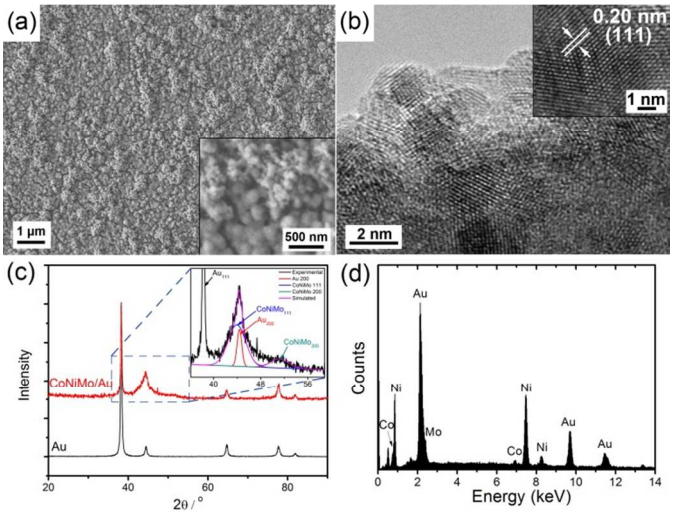

Figure 3. (a): SEM image of CoNiMo layer (top view); the inset is the SEM image at a higher magnification; (b): TEM and HRTEM images of the scraped CoNiMo layer showing crystalline species; (c): GIXRD pattern of the CoNiMo thin film on Au disk; (d): energy-dispersive X-ray spectrum obtained using the EDS detector on the SEM.

The HOR in an alkaline medium proceeds through the following reactions by either Tafel-Volmer or Heyrovsky-Volmer squences:[35]

$$H_2 + 2* \leftrightarrow 2H_{ad} \quad \text{(Tafel)}$$
$$H_2 + OH^- + * \leftrightarrow H_{ad} + H_2O + e^- \quad \text{(Heyrovsky)}$$
$$H_{ad} + OH^- \leftrightarrow H_2O + e^- + * \quad \text{(Volmer)}$$

As seen from the above elementary steps, the adsorption and binding strength of H play a critical role in determining the HOR activity in alkaline electrolyte, as suggested through the reverse reaction HER in our previous work on polycrystalline mono-metallic catalyst systems.[37] To probe qualitatively if HBE also plays an important role in this multi-metallic catalyst system, hydrogen binding energy (HBE) values were calculated using DFT method on structurally simpler model surfaces, and parallel H_2-TPD measurements were also carried out. DFT calculations show that Ni(111) and Mo(110) have notably higher HBEs than Pt(111), NiMo exhibits much lower HBE than Ni and Mo, and CoNiMo possesses an HBE value between those of NiMo and Pt (Table 2). The HBE trend calculated from DFT is consistent with the H_2-TPD measurements (Fig. S4) in that Ni and CoNi modified Mo(110) surfaces show lower desorption temperatures than the clean Ni(111) surface. Strmcnic et al.[14] suggest that adsorbed OH species on the catalyst surface may facilitate the overall HOR activity, although OH_{ad} species are not directly shown in the elementary reaction steps. It is noted from the Pourbaix diagram that in the vicinity of the reversible hydrogen potential, Co and Ni exist in the form of hydroxides. However, it is unlikely that these OH species would dominate the HOR activity as NiMo demonstrates markedly enhanced HOR activity over Ni, while both should have similar surface coverage of OH. Thus, the HBE values appear to be critical in controlling the HOR activity for the catalysts used in the current study.

Table 2. Hydrogen binding energies from DFT calculations for the most energetically favorable binding site for each surface.

	Mo (110)	Ni (111)	Ni_{ML}/Mo (110)	CoNi/Mo (110)	Pt (111)
Binding Energy (eV)	−0.70	−0.51	−0.40	−0.43	−0.46
Binding Energy (kJ/mol)	−67.6	−49.5	−38.6	−41.6	−44.7
Binding Site	bridge	fcc	bridge	bridge	fcc
Bond Length (Å)	1.90	1.71	1.64	1.66	1.87
Bond Angle	44.8	42.5	38.4	37.7	39.0

Conclusions

In conclusion, we have synthesized a highly active precious-metal-free Ni-based HOR electrocatalyst. Our results suggest that the specific HOR activity of CoNiMo is 20 times higher than Ni in alkaline medium. The remarkably enhanced activity is ascribed to the weakened hydrogen binding energy on CoNiMo. This innovative material can potentially mitigate the catalyst cost issue by providing a pathway to non-precious metal catalysts as viable replacement to Pt at the anode of alkaline or alkaline membrane fuel cells.

Acknowledgements

This work is supported by the US Department of Energy (DE-FG02-13ER16381 and ARPE (DE-AR0000009). We would like to thank Prof. Michael Mackay, Mr. Brian McCandless and Mr. Ngoc A. Nguyen for the GIXRD measurements and Ms. Jie Zheng for the assistance in the SEM characterization.

Notes and references

[1]Department of Chemical and Biomolecular Engineering, and Center for Catalytic Science and Technology, University of Delaware, Newark, DE 19716
[2]Department of Chemical Engineering, Columbia University, New York, NY 10027
[3]Chemistry Department, Brookhaven National Laboratory, Upton, NY 11973

Electronic Supplementary Information (ESI) available: H_2-TPD spectrum, SEM and HRTEM images of CoNiMo catalyst layer, Butler-Volmer fitting of the HER/HOR currents on Pt and CoNiMo, and cyclic voltammograms of Pt and CoNiMo. See DOI: 10.1039/b000000x/

1. H. A. Gasteiger, S. S. Kocha, B. Sompalli and F. T. Wagner, *Appl Catal B-Environ*, 2005, 56, 9-35.
2. H. A. Gasteiger and N. M. Markovic, *Science*, 2009, 324, 48-49.
3. R. F. Service, *Science*, 2009, 324, 1257-1259.
4. W. Gu, D. R. Baker, Y. Liu and H. A. Gasteiger, in *Handbook of Fuel Cells: Fundamentals, Technology and Applications*, eds. W. Vielstich, H. A. Gasteiger and H. Yokokawa, John Wiley& Sons, Chichester, 2009, vol. 6, pp. 631-657.
5. R. Borup, J. Meyers, B. Pivovar, Y. S. Kim, R. Mukundan, N. Garland, D. Myers, M. Wilson, F. Garzon, D. Wood, P. Zelenay, K. More, K. Stroh, T. Zawodzinski, J. Boncella, J. E. McGrath, M. Inaba, K. Miyatake, M. Hori, K. Ota, Z. Ogumi, S. Miyata, A. Nishikata, Z. Siroma, Y. Uchimoto, K. Yasuda, K. I. Kimijima and N. Iwashita, *Chem Rev*, 2007, 107, 3904-3951.
6. Y. Shao-Horn, W. C. Sheng, S. Chen, P. J. Ferreira, E. F. Holby and D. Morgan, *Top Catal*, 2007, 46, 285-305.
7. M. Lefevre, E. Proietti, F. Jaouen and J. P. Dodelet, *Science*, 2009, 324, 71-74.
8. G. Wu, K. L. More, C. M. Johnston and P. Zelenay, *Science*, 2011, 332, 443-447.
9. H. Meng, F. Jaouen, E. Proietti, M. Lefevre and J. P. Dodelet, *Electrochem Commun*, 2009, 11, 1986-1989.
10. H. T. Chung, J. H. Won and P. Zelenay, *Nature Communications*, 2013.
11. J. Suntivich, H. A. Gasteiger, N. Yabuuchi, H. Nakanishi, J. B. Goodenough and Y. Shao-Horn, *Nat Chem*, 2011, 3, 546-550.
12. N. M. Markovic, S. T. Sarraf, H. A. Gasteiger and P. N. Ross, *J Chem Soc Faraday T*, 1996, 92, 3719-3725.
13. W. C. Sheng, H. A. Gasteiger and Y. Shao-Horn, *J Electrochem Soc*, 2010, 157, B1529-B1536.
14. D. Strmcnik, M. Uchimura, C. Wang, R. Subbaraman, N. Danilovic, D. van der Vliet, A. P. Paulikas, V. R. Stamenkovic and N. M. Markovic, *Nat Chem*, 2013, 5, 300-306.
15. L. L. Chen and A. Lasia, *J Electrochem Soc*, 1992, 139, 3458-3464.
16. P. W. Du and R. Eisenberg, *Energ Environ Sci*, 2012, 5, 6012-6021.
17. C. L. Fan, D. L. Piron, A. Sleb and P. Paradis, *J Electrochem Soc*, 1994, 141, 382-387.
18. J. Y. Huot, M. L. Trudeau and R. Schulz, *J Electrochem Soc*, 1991, 138, 1316-1321.
19. I. A. Raj and K. I. Vasu, *J Appl Electrochem*, 1992, 22, 471-477.
20. P. D. Tran, S. Y. Chiam, P. P. Boix, Y. Ren, S. S. Pramana, J. Fize, V. Artero and J. Barber, *Energ Environ Sci*, 2013, 6, 2452-2459.
21. K. Strasser, *J Electrochem Soc*, 1980, 127, 2172-2177.
22. Y. Kiros and S. Schwartz, *J Power Sources*, 2000, 87, 101-105.
23. T. Kenjo, *J Electrochem Soc*, 1985, 132, 383-386.
24. K. Mund, G. Richter and F. V. Sturm, *J Electrochem Soc*, 1977, 124, 1-6.
25. H. Tanaka, N. Kaneki, H. Hara, K. Shimada and T. Takeuchi, *Can J Chem Eng*, 1986, 64, 267-271.
26. W. Jenseit, A. Khalil and H. Wendt, *J Appl Electrochem*, 1990, 20, 893-900.
27. D. E. Brown, M. N. Mahmood, M. C. M. Man and A. K. Turner, *Electrochim Acta*, 1984, 29, 1551-1556.
28. C. L. Fan, D. L. Piron and M. Rojas, *Int J Hydrogen Energ*, 1994, 19, 29-33.
29. I. A. Raj and K. I. Vasu, *J Appl Electrochem*, 1990, 20, 32-38.

30. S. F. Lu, J. Pan, A. B. Huang, L. Zhuang and J. T. Lu, *P Natl Acad Sci USA*, 2008, 105, 20611-20614.
31. G. Kresse and J. Furthmuller, *Comput. Mater. Sci.*, 1996, 6, 15-50.
32. G. Kresse and J. Hafner, *Phys. Rev. B*, 1993, 47, 558-561.
33. J. K. Norskov, T. Bligaard, A. Logadottir, J. R. Kitchin, J. G. Chen and S. Pandelov, *J Electrochem Soc*, 2005, 152, J23-J26.
34. A. J. Bard and L. R. Faulkner, *Electrochemical Methods: Fundamentals and Applications*, John Wiley & Sons, New York, 2001.
35. K. J. Vetter, *Electrochemical Kietics: Theoretical and Experimental Aspects*, Academic Press, New York, 1967.
36. C. L. Fan, D. L. Piron and P. Paradis, *Electrochim Acta*, 1994, 39, 2715-2722.
37. W. C. Sheng, M. Myint, J. G. G. Chen and Y. S. Yan, *Energ Environ Sci*, 2013, 6, 1509-1512.